2013

A study in merger induced galaxy evolution through post-starburst systems

Zachary Dean Griffith
University of Northern Iowa

A STUDY IN MERGER INDUCED GALAXY EVOLUTION THROUGH POST-STARBURST SYSTEMS

A Thesis Submitted

in Partial Fulfillment

of the Requirements for the Designation

University Honors with Distinction

Zachary Dean Griffith

University of Northern Iowa

May 2013

Abstract

We discuss an optical study of a triple galaxy system at a redshift of 0.06. In optical images from Data Release 7 of the Sloan Digital Sky Survey (SDSS), the system consists of a close pair plus another galaxy at a projected distance of 35 kpc. Tidal features extending at least 30 kpc are visible to the southeast of both the galaxy pair and the third member of the system, suggesting significant interaction. One of the the pair and the more isolated galaxy are low-luminosity radio sources. The lone galaxy appears extended in a radio map from the FIRST survey. If the radio emission arises from ongoing star formation, the implied star formation rates are 1 to 2 solar masses per year in each source. We have acquired deep spatially resolved optical (3500-8500 Å) spectroscopy with the Sparsepak integral field unit and the Bench Spectrograph on the WIYN 3.5-meter telescope. Both the pair and the more isolated galaxy show post-starburst (K+A) spectral signatures, and stellar population synthesis using Bruzual and Charlot (2003) models indicate that all components of the triple system had episodes of significant star formation at comparable times in the past. This system is part of a larger study of post-starburst galaxies which host radio sources that potentially indicate the presence of an active galactic nucleus (AGN). The goals of this study include a better understanding of the connection between, and relative timing of, galaxy interactions and the triggering of star formation and an active galactic nucleus.

1 Introduction

When galaxies that have a similar mass collide, they evolve through certain phases of what is called a major merger. Based on current merger models and observations, this evolutionary process is thought to proceed in the following way: As the galaxies coalesce, there is a large scale influx of gas towards the center, driving nuclear star formation and accretion onto the central supermassive black hole. Following this, intense AGN activity dominates the luminosity, but is likely obscured by surrounding gas and dust, as the black hole at the center of the system grows quickly. Feedback due to the black hole's accretion energy into surrounding gas and supernovae from newly formed massive stars causes gas and dust to be expelled from the center of the system. This removes the obscuring material from the center and reveals the phase of traditional quasar activity (extreme luminosity) for the AGN. As the remaining central gas is blown out or used up, the fuel for both star formation and AGN activity is depleted. The luminosity of the AGN fades and the spectrum

of the galaxy reddens after star formation is rapidly truncated. For the next few hundred million years, the merged galaxy exists in a post-starburst phase with a specific spectral signiture. The luminosity continues to fade and redden, finally ending in a quiescent red elliptical galaxy (a galaxy with no star formation and an elliptical shape) (Hopkins et al. 2008).

This thesis focuses on the post-starburst phase of galaxy evolution. Post-starburst galaxies are also called K+A galaxies, as their spectral signature includes a combination of K-type stars associated with older elliptical galaxies and A-type stars associated with recent star formation (Poggianti et al. 1999). However, the spectra of traditional post-starburst galaxies have no optical emission lines, which means there is no current or ongoing star formation. The galaxies in this study were chosen from a sample of post-starburst galaxies originally selected based on their nuclear spectra from the SDSS. These were determined using the spectral characteristics of a post-starburst: the equivalent width of the Hδ absorption line is greater than 4 Å, the equivalent width of the [OII] emission line is greater than -2.5 Å, and the equivalent width of the Hα absorption line is greater than -3.5 Å (Goto 2007). In addition, the galaxies of this study are among a small subset ($\sim$3 percent) of the sample that display radio properties, determined using the NRAO VLA Sky Survey (NVSS) and Faint Images of the Radio Sky at Twenty-cm (FIRST) radio surveys, which suggest ongoing or recent AGN activity after the galaxies have largely stopped forming stars. This phenomenon suggests that we might be observing galaxies with AGN that are in the final fading stages of once powerful quasars.

Among the galaxies chosen to be analyzed, one system has proven to be particularly interesting, and was the focus of much of this research. It is a triple galaxy system, consisting of a galaxy pair in the post-starburst phase and a nearby galaxy at a projected distance of 35 kpc. The galaxy pair has the standard coordinate name J075323.0+243300, but for the sake of clarity in this paper the galaxies will be referred to as "pair A," "pair B," and the companion; these are shown in Figure 1a. Tidal features extending at least 30 kpc are visible to the southeast of both the galaxy pair and the third member of the system, suggesting significant interaction has occurred. Figure 1b is an image from the FIRST survey that shows both pair B and the more isolated galaxy are low-luminosity radio sources. Pair B is a point source of 2.9 mJy in FIRST, while the companion galaxy is an extended source in FIRST with an integrated flux density of 3.0 mJy. These two sources blended together in the much lower resolution NVSS, which detected a single point source of 4.1 $\pm$ 0.4 mJy.

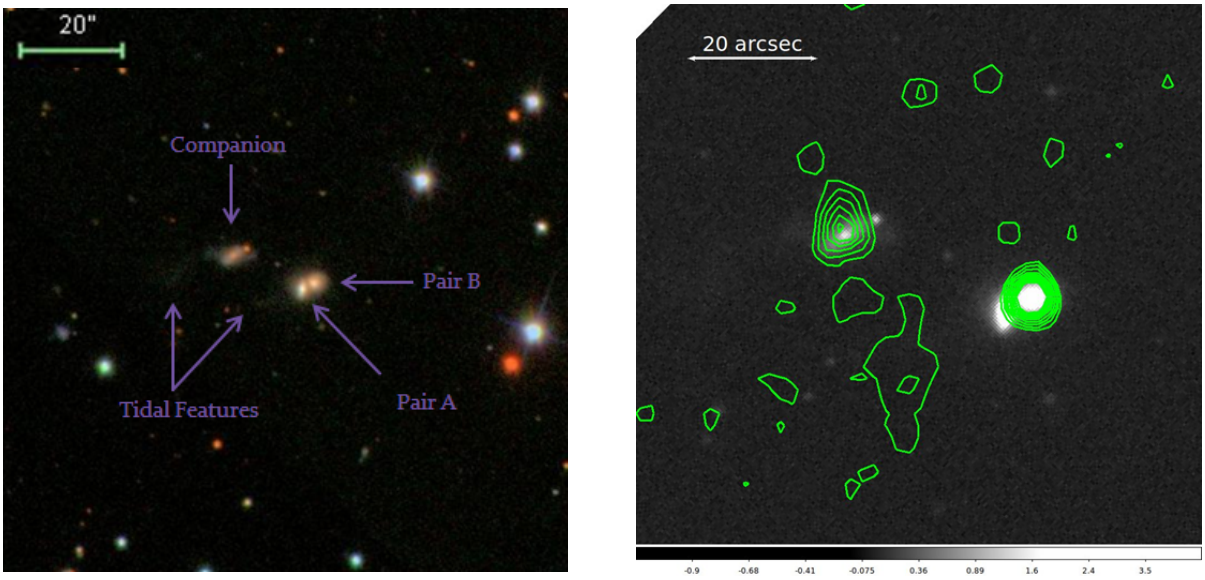

(a) Optical Image from SDSS DR7

(b) Radio Image from the FIRST Survey

Figure 1: Images of the J075323 System

The difference between the FIRST and NVSS surveys indicates possible variability in either one or both of the sources. This combined with the extended source of the companion may be an indicator of AGN activity.

An additional galaxy, J233917.8-001457, was selected for observation. Figure 2 shows the SDSS optical image of the galaxy, which has a redshift of 0.069. This galaxy is also a post-starburst and a radio source designated by FIRST and NVSS. However, whether the most recent starburst in this galaxy was merger-induced was more difficult to determine from the SDSS image alone.

2 Purpose

This study seeks to provide empirical evidence for or against a collision scenario between the galaxy pair and companion of the system J075323. Additionally, we will distinguish the source of emission from the galaxies as either star formation or AGN activity, as well as identify any possible gas outflows.

3 Literature Review

Post-starburst galaxies can be produced by several different mechanisms, but a significant fraction of them are created via the merger of two or more gas-rich galaxies. Pracy et al. (2005) analyzed 10 nearby (z = 0.04-0.20) post-starburst galaxies from the Two Degree Field Galaxy Redshift Survey using data from the Gemini Multi Object Spectrograph (GMOS), which is an integral field unit (IFU). Of these, seven showed tidal features. Tidal features are drawn out or distorted parts of a galaxy caused by tidal forces by the gravitational field of galaxies. Tidal features and disturbed morphologies are clear evidence of interaction or merging between galactic bodies. Additional studies have supported the idea that a significant fraction of post-starburst galaxies are the product of gas-rich galaxy mergers (Zabludoff et al. 1996; Chang et. al 2001; Yang et al. 2008).

Overall, post-starburst galaxies have relatively blue spectral signatures, indicating that the light from recent star formation is more prominent than that of the other, much older star formation episodes associated with K-type stars. However, the color distributions and gradients of post-starbursts can vary depending on where the starbursts occurred. Color distribution refers to the amount of red (associated with older stars) and blue (associated with newer stars) dispersion over regions of the galaxy. Color gradients refer to the change from red to blue (a positive gradient) or blue to red (negative gradient) going from the outer edge of the galaxy in towards the nucleus. Modeling of post-starburst galaxies has suggested that star formation should be centered in the core of the galaxies as a product of the gas funneled there during the merger (Hopkins et al. 2008, Snyder et al. 2011). However, the aforementioned analysis done by Pracy et al. (2005) found that post-starburst galaxies can have red, blue, or irregular cores, and have negative, flat, or positive color gradients. Yamauchi and Goto (2005) reported similar varied behavior in post-starbursts. Yang et al. (2008) analyzed 21 post-starburst galaxies using high-resolution data from the Hubble Space Telescope's Wide-Field Planetary Camera 2 and Advanced Camera for Surveys. While they also concluded the color distributions to be diverse, they found that 70 percent of their sample had a positive color gradient, which indicates that the younger stellar populations are more concentrated than the old (Yang et al. 2008).

A more recent study by Pracy et al. (2012) involved a sample of post-starburst galaxies from the Sloan Digital Sky Survey (SDSS) selected for their very low redshift (z < .01). This corresponds to

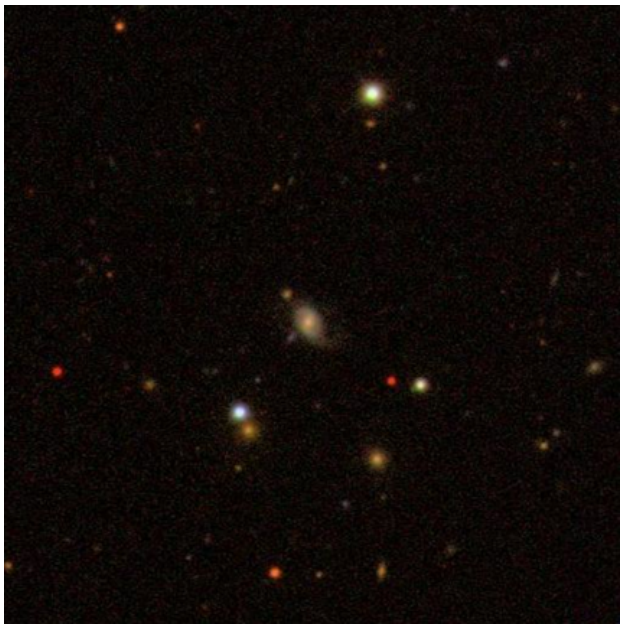

Figure 2: An SDSS image of the galaxy J233917.8-001457.

an angular scale of ∼0.18 kpc per arcsecond. They took data using the Wide Field Spectrograph (WiFeS) on the Australian National University's 2.3-m telescope. WiFeS has a spatial resolution of 1 arcsecond per fiber. This allowed the team to easily resolve the inner ∼1 kpc of the galaxies and analyze the color distribution. In contrast, the triple galaxy system focused on in this study has a redshift of z = ∼0.061. This correlates to a scale of 1.138 kpc per arcsecond in the sky. The width of the binary galaxies at their broadest point is ∼12 kpc, or a little more than 10 arcseconds across. SparsePak fibers are 5 arcseconds across each, so at this redshift spatial resolution is limited and analysis of star formation specific to the nucleus is impossible. However, we can explore general trends in whether younger stars exist in areas of close proximity of the pair or on the outer edges to suggest a possible interaction theory. Using equivalent width measurements, Pracy et al. (2012) found that the post-starburst regions were centrally concentrated and contained within the inner ∼1 kpc of the galaxies. This supports the modeling work done on post-starbursts (Hopkins et al. 2008; Snyder et al. 2011).

Another property of post-starburst galaxies is the amount of evident rotation by the young stellar populations. There have been two major studies conducted that analyzed the rotation of low redshift post-starburst galaxies, with each finding quite different results. Norton et al. (2001) conducted a study using long slit spectroscopy that yielded little to no evidence for rotation. In the other study,

Pracy et al. (2009) found that the young stellar populations displayed significant rotation. These contradictory reports might be explained by the possibility that the axis of rotation in these galaxies does not line up with the isophotal major axis. In this case, data taken using a one-dimensional long slit, as Norten et al. (2001) used, would yield lessened or suppressed amounts of rotation. As mentioned, Pracy et al. (2005) used GMOS, an IFU, which avoids this complication due to better spacial sampling of the galaxy.

The "lifetime" of post-starburst galaxies is measured by the time elapsed since significant star formation ceased. The canonical lifetime of post-starburst galaxies has been the lifetime of an A-type star, which ranges from 500 million years to 1.5 billion years. Since A-type stars are the product of recent star formation, it stands to reason that the age of these stars age-date the post-starburst phases. However, this number is subject to contention. Snyder et al. (2011) ran simulations of galaxy mergers to model post-starburst galaxies and get an estimate of their lifetimes. These simulations produced a mean post-starburst lifetime of around 200 million years, with systems exceeding 300 million years only around half the time. They also concluded that the only long-lived, billion year old post-starbursts are those that experience a very strong and fast starburst, which is ideal for producing post-starburst spectral features (Snyder et al. 2011). However, most observational studies have determined that post-starburst galaxies have lifetimes consistent with the $\sim$1 billion years figure, possibly suggesting an observational bias toward these longer lived signatures.

The properties discussed so far (and the studies analyzing them) have dealt with pure post-starburst galaxies which, as mentioned, should have a relatively dormant nucleus. However, observations have suggested that some galaxies have properties consistant with a post-starburst, yet show weak activity in the AGN. One such body is the galaxy G515. This galaxy was first observed by Oegerle et al. in 1991, at which time there was no evidence for AGN activity. The galaxy's extremely high luminosity (determined to be $\sim 10^{12}$ times the luminosity of the Sun at the galaxy's peak luminosity) led Oegerle et al. (1991) to propose that it was formerly an ultra-luminous infrared galaxy (ULIRG). This galaxy was revisited by Liu et al. in 2007, who found that data from the FIRST radio survey showed no significant radio activity, while data from the NVSS radio survey did. This variable radio activity was proposed by Liu et al. (2007) to be the consequence of the galaxy's past life as a ULIRG, supporting Oegerle et al.'s hypothesis. Comparisons of other galaxies

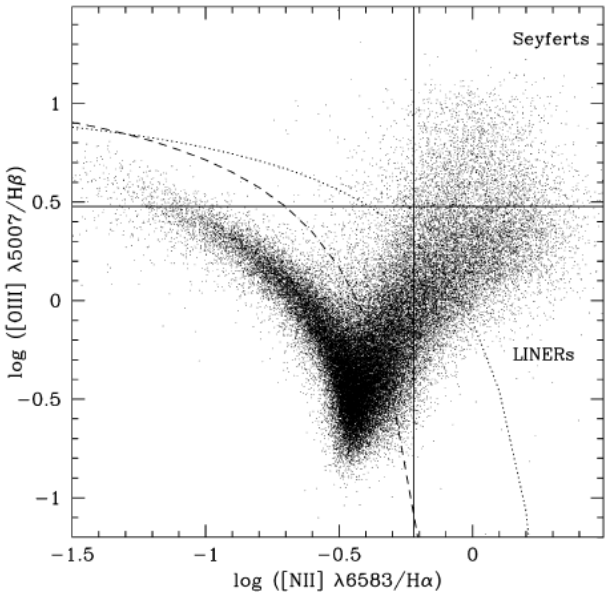

Figure 3: An example BPT Diagram (Kauffman et al. 2003).

in the post-starburst sample of the SDSS using NVSS and FIRST data has yielded a small subset of galaxies with steady or variable AGN in the same vein as G515. This subset of galaxies was analyzed in this study.

Some of the galaxies from this project's sample have emission lines in the optical spectrum of regions outside the nucleus. These emission lines have two main causes: star formation or AGN activity. Baldwin, Phillips, and Terlevich (1981) pioneered a technique which compares two ratios for emission line analysis. The first ratio was [OIII] (the intensity of the OIII emission line, which has a rest wavelength of 500.7 Å) over the recombination line Hβ. The second was [NII] (the intensity of the NII emission line, which has a rest wavelength of 6584 Å) over the recombination line Hα (Baldwin et al. 1981). The plot of [OIII]/Hβ vs [NII]/Hα is known as a BPT diagram, from the authors' names (Baldwin, Phillips, and Terlevich). The location of a galaxy on this diagram can be used to infer whether the emission lines are caused by ionization from an AGN (BPT-AGN) or from star formation (BPT-SF). Two major studies are often referenced that provide a curve on the BPT diagram that divides BPT-AGN and BPT-SF galaxies. The first used modeling of infrared starburst galaxies to derive a theoretical division (Kewley et al. 2001). The second used observational data from the SDSS to determine a division (Kauffmann et al. 2003). Galaxies that fall in the area between the two curves are designated as composite galaxies (BPT-comp). One

hinderance of the BPT diagram is that it can only be utilized for galaxies of redshift z<0.5, as the [NII] emission line is redshifted out of the optical spectrum at any higher value (Trouille et al. 2011). An alternative emission line analysis method has been proposed by Trouille, Barger, and Tremonti (2011). They plot the rest frame g - z color against the log of the ratio of the NeIII and OII doublet emission line intensities. This diagram (called a TBT diagram) can be used for galaxies out to z=1.4 (Trouille et al. 2011).

Theoretical models of merger galaxies that used star formation as the sole feedback mechanism when the galaxies merged resulted in galaxies that are too luminous in the post-starburst phase compared to observations (Croton et al. 2006; Bower et al. 2006). To counteract this, new models included quasar feedback as a method of quickly ending the starburst period and thus producing a galaxy with redder features (Granato et al. 2004; Springel, Di Matteo, Hernquist 2005; Hopkins et al. 2006). Such AGN feedback should result in galactic outflows due to stellar winds that have significantly greater velocities than outflows driven by supernovae commonly seen from starburst galaxies (Thacker, Scannapieco Couchman 2006). Tremonti, Diamond-Stanic, and Moustakas (2009) found nearly two-thirds of a sample of 35 post-starburst galaxies produced large outflow velocities in agreement with quasar-feedback models.

4 Instrumentation

The data analyzed in this study consists of deep optical spatially resolved spectra taken of post-starburst galaxies using the SparsePak integral field unit (IFU) on the WIYN 3.5 meter telescope. SparsePak is a fiber-optic bundle consisting of 82 fibers, each five arcseconds in diameter. These fibers, shown in Figure 4 are arranged in a unique formation, with a densly packed central core of seventeen fibers to maximize spatial sampling in the center of a galaxy, a surrounding sparse region of 58 fibers that enables sampling over larger areas of the sky, and an outer boundary of seven additional fibers that measure sky light for the purpose of data reduction. IFUs such as SparsePak offer advantages in spatial resolution and observation speed over traditional long slit spectroscopy. Long slit spectrographs take in light through a single slit, which is then stepped along the imaged area until all the desired spectra are obtained. In contrast, IFUs can obtain many spectra simultaneously in a two-dimensional field. Figure 5 shows the SparsePak fiber “map”

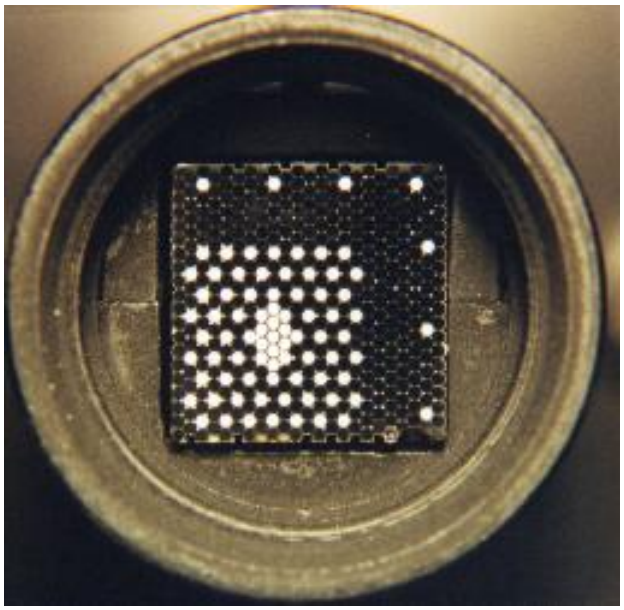

Figure 4: The SparsePak Fiberhead.

overlaid on the image of the J075323 system (Bershedy et al. 2004).

When an image is taken, the light is collected by each fiber simultaneously, then read into the bench spectrograph. The bench spectrograph aligns the fibers into a single slit, which passes through a collimator and diffraction grating to seperate the light into spectra. To get a complete coverage range, images were obtained at two wavelength regions, a "blue" spectrum spanning from ∼3800 Å to ∼6600 Å and a "red" spectrum from ∼6400 Å to ∼9000 Å. The two wavelength ranges are then combined during the data reduction prcoess. These images were taken in half hour exposure increments, with totals of four hours of coverage in the blue and six hours in the red for the galaxy system J075323 (Bershedy et al. 2004).

5 Methods

5.1 Data Reduction

While IFUs offer several advantages over long split spectroscopy in data collection, they also considerably complicate the data reduction process.

The procedure began with the data in its raw, unprocessed state. At this stage, each image was

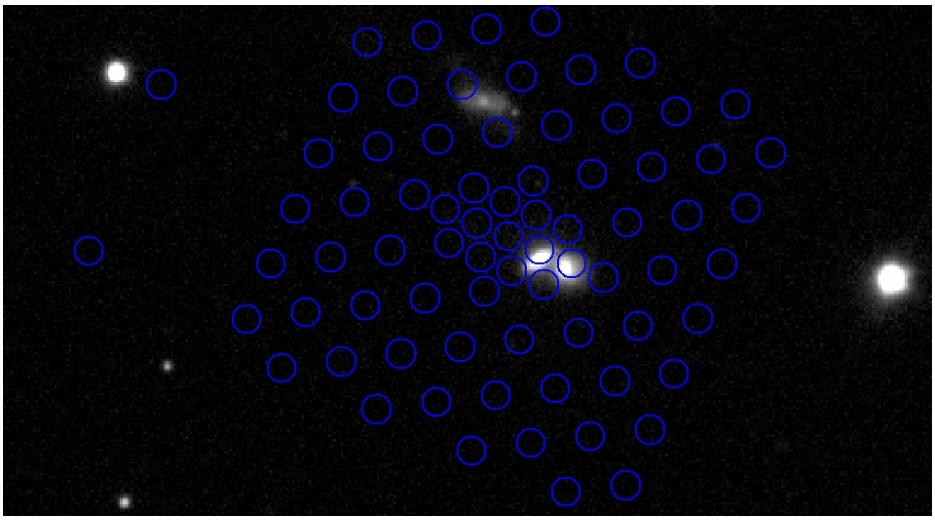

Figure 5: The SparsePak Fiber Map overlaid on J075323.

a series of 82 columns, with each column corresponding to a spectrum for a fiber. Each row in the column corresponded to a wavelength value, and the intensity of each pixel represented the flux at that particular wavelength. The first step was to remove structure along the columns that accumulated from reading the image out from the spectrograph. This structure was purely electronic in nature, and was compensated for by an overscan region in the image. As this region was outside the illuminated part of the detector, the signal present was entirely electronic. This was averaged and subtracted from the rest of the image to account for the electronic structure. Once the correction was done, the overscan portion of the image was trimmed off.

Next, the electronic noise introduced by the charged coupling device (CCD) camera (the collector for the light off the diffraction grating) was reduced. This was done using zero frames, which are images taken with a zero second exposure. Averaging the results of many of the zero frames (usually $\sim$50) gives a composite noise frame which was subtracted from the rest of the images.

In addition to the two dimensional electronic structure, the CCD introduced additional unwanted signal due to electrons that are thermally produced during an exposure. To correct for this, images of the same exposure duration as object images (thirty minutes) were taken with the shutter of the telescope closed. All of these "dark frames" from an observing run were averaged together to make a composite frame. Due to the relatively small amount of signal that was produced from this effect, dark frame subtraction was not necessary for the shorter exposure object frames.

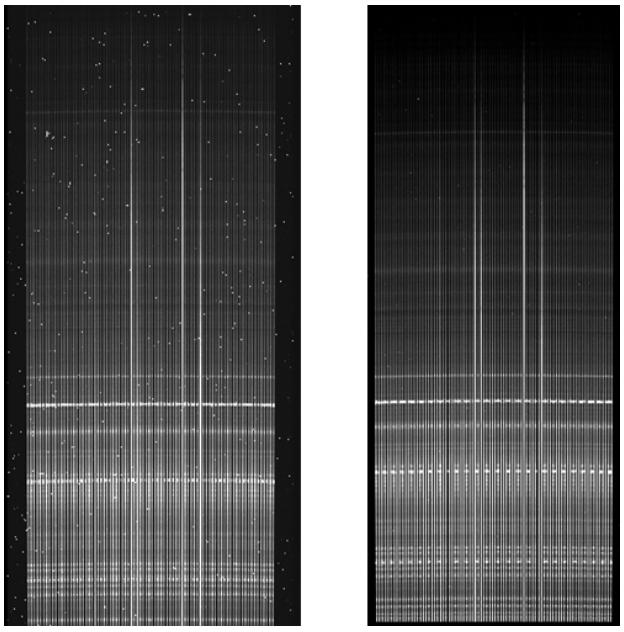

Figure 6: On the left is a spectrum before cosmic ray reduction, while the right shows the spectrum afterwards.

Cosmic rays were another unavoidable addition to the signal that had to be removed. In most cases, this was accomplished by combining two object images together. With the right parameters accounting for discrepency, the large increases in signal caused by cosmic rays that were present in one frame but not in the other were correctly identified and taken out of the combined image. However, in some cases this was either inadequate or the parameter settings for discrepancies needed to be set too high, resulting in loss of signal from the objects. In these cases, the object frames in question were ran through a cosmic ray reduction procedure individually. Figure 6 shows the results of cosmic ray reduction.

The next step was extracting the spectra from the fibers. This process involved several steps which are combined into a single procedure called dohydra. First, the fibers that actually covered the galaxy were designated, while those that did not collect any galaxy light were used for sky subtraction. Next, the pixel to pixel sensitivity variations were corrected for. This accounts for the fact that the CCD pixels were not uniform. This is accomplished using dome "flat frames", which are images of a blank screen in the observatory. As ideally there would be no variations, any discrepancies from pixel to pixel in these dome flat images were used to correct for variance in pixel sensitivities. After flat fielding, it was necessary to find the dispersion solution, which translates the

pixel numbers to wavelength values. This is done by taking images of a CuAr (copper-argon) lamp during observation. This lamp has very well defined spectral emission lines at certain wavelengths. Thus, comparing CuAr lamp images to an accepted image using these spectral features allowed a pixel-to-wavelength conversion. Finally, sky features were subtracted from the spectra. Using the light from fibers samplin blank sky in object frames, a composite spectrum of the sky was produced and subtract off of the galaxy spectra.

Extracted spectra were then ran through fiber-to-fiber throughput correction. This was done using sky flats: images of the sky at twilight, where the Sun illuminates the sky evenly. Sky flats offered several advantages over dome flats for this step. Namely, sky light enters the telescope at the same angle as the galaxy light, which is not possible for light off of the illuminated dome screen. Additionally, sky light is more even in signal across the spectrum than dome lamp light, especially on the blue end, where dome lamp light drops off and does not yield a sufficient signal-to-noise ratio. Fiber-to-fiber throughput correction was necessary to achieve the greatest accuracy in the final step of the data reduction process: flux calibration. This correction accounts for varying wavelength dependent throughput in different optical fibers.

Flux calibration corrected for an average extinction and removed the instrumental response function from galaxy spectra. This was accomplished by taking images of a "standard star", a star that has had its light output thoroughly and precisely measured. By comparing the images taken during the observing run to the accepted characteristics, flux calibration was accomplished and applied to all galaxy spectra.

5.2 Stellar Population Synthesis

The spectrum of a galaxy is a combination of the spectra of all the stars that inhabit it. Certain populations of stars will dominate galaxy light; these are known as single stellar poulations, and each has a particular age associated with them. The spectra of these stars are compiled in a stellar population library. Some combination of stars from the stellar population library produces the most accurate model of the galaxy light we observe. The ages of the stars that are used in this model yield information about when the star formation periods, or starbursts, occurred in the galaxy. This is stellar population synthesis; the primary method of analysis used in this paper. Figure 7 shows

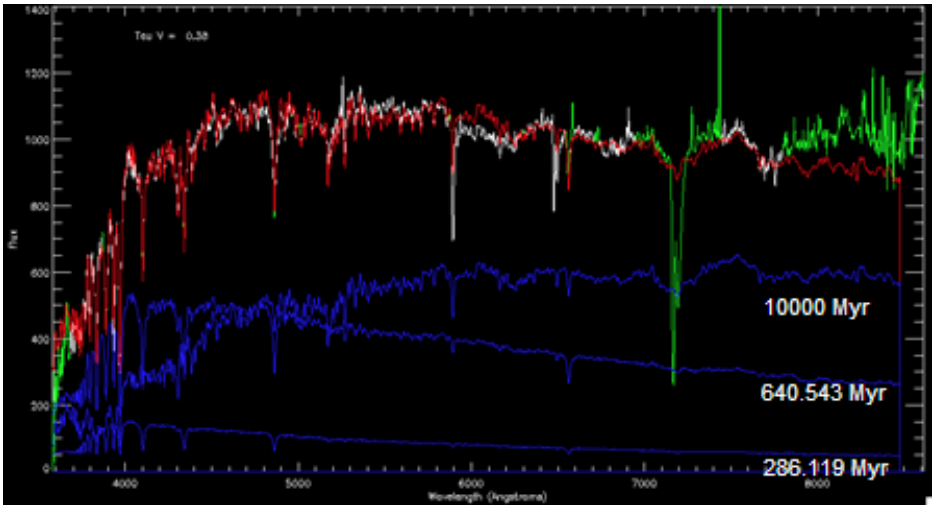

Figure 7: An example output of stellar population synthesis.

an example output of the stellar population code. There are several different components to the image. The white spectrum is the actual data. The red spectrum is the model fit, a combination of several single stellar populations. The green regions are those masked out from the modeling process. Masking is done for several reasons. Instrumental limitations lead to a loss in signal in the blue, making model fitting not feasable. In the long wavelength regime, sky features become more and more prominent. Absorption lines that are caused by atmospheric features must be removed. Finally, emission lines are not accounted for in the stellar population fit. The blue spectra are those of the stellar populations that comprise the composite model fit.

There are several different libraries of model stars available. We used the library constructed by Bruzual and Charlot (2003). The subset of this library that we utilized consists of ten single stellar populations, ranging in age from the youngest at just over five million years to the oldest at ten billion years. Before discussing results, it is important to note that stellar population synthesis still has some limitations. Phases of stellar evolution such as the asymptotic giant branch and supergiant phases are relatively poorly understood. The short life span of these stars, combined with their brightness, means that mass loss is vital to correctly construct their evolutionary path. The high degree in difficulty of modeling mass loss introduces a fair amount of uncertainty. Additionally, changing age and metallicity in populations has similar effects: increasing metallicity raises opacity in stars, which reddens the spectrum. Aging stars also reddens the spectrum. Thus, a low-metallicity, old stellar population can have a spectrum almost identical to that of a

high-metallicity, young stellar population. This is known as age-metallicity degeneracy, and is an ever-present quandary in the stellar population synthesis. All this being said, stellar population snythesis is still a very effective method of deriving information on the stellar age groups in galaxies.

6 Results

6.1 J075323

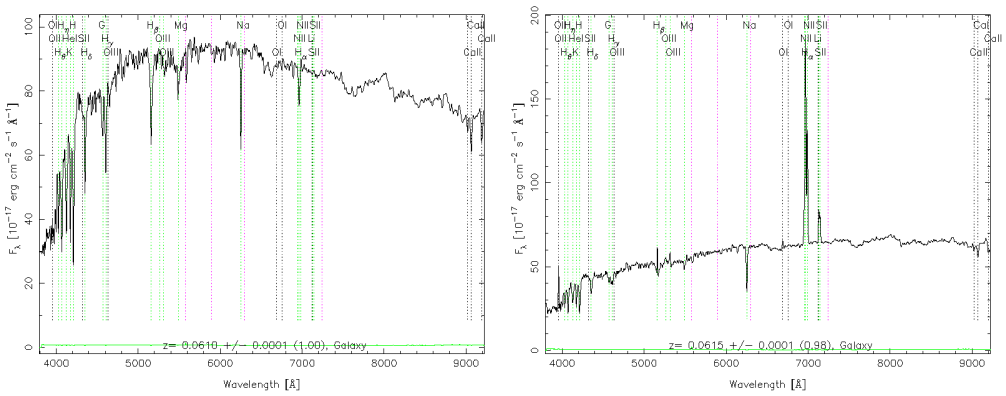

Figure 8: Spectra of the nuclei of the galaxy pair. Pair A is on the left, while Pair B is on the right.

Figure 12 shows the results of stellar population synthesis for the J075323 system. There are five spectra labeled with fiber numbers which correspond to the data gathered using SparsePak. Additionally, there are two spectra from the SDSS. These are taken at the nucleus of their respective galaxies. Table 3 shows the percentage of total light that each stellar population produces for a particular spectrum.

An important theme to note among the spectra is the prevalence of major stellar populations in three age groups: 286.12 million years, 640.54 million years, and 904.79 million years. A system with significant recent star formation of less than a billion years, but little current star formation indicates a major merger at some point in the past. In addition, all fibers on the galaxy pair have substantial older stellar populations. The combination of these two features supports the designation of this system as post-starburst

Out of the seven spectra, only fiber 46 has no significant populations in any of these groups. An

Table 1: Emission line fitting results for J075323 system.

	Emission Line Flux			
	[OIII] λ5007	Hβ	[NII] λ6584	Hα
Fiber 25	342.36	378.91	2570.62	3396.05
Fiber 31	362.84	68.79	1080.39	994.18
Fiber 46	90.55	-33.82	193.94	70.01
Fiber 48	1195.83	3342.57	11614.70	22797.20
Fiber 60	76.82	206.20	542.68	987.645
SDSS Pair A	35.61	-64.75	86.29	29.60
SDSS Pair B	69.72	194.52	959.4	1745.6

explanation may lie in Figure 1a, which shows a dark region betwen the galaxy pair, a potential major area of interaction in their area of closest proximity. From the overlaid fiber map at the center of Figure 12, we see that fiber 46 lies well outside that interaction area, placed solely on the outside of galaxy pair A. No recent star formation in this area supports that there has been little interaction with galaxy pair B in the system in this area.

Relatively current star formation is shown through the presence of the 5.01 million year and 25.12 million year stellar populations. Fiber 48 and the SDSS nuclear spectrum for pair B both show signficant light percentages contributed by these stellar populations, while fiber 25 shows a small contribution (5.21 percent) from the 25.12 million year stellar population. The fiber map from Figure 12 shows that fiber 48 is entirely on pair B (almost to the same extent as the SDSS nuclear spectra) and fiber 25 is partly on fiber A and partly on fiber B. Thus, we conclude that pair B has substantial current star formation. This may contribute significantly towards its radio emission seen in Figure 1b.

Fiber 60 is placed on the companion galaxy. This galaxy also shows evidence of recent star formation, with stellar populations of 286.12 million years and 640.54 million years contributing to the fit. Additionally, it has an older epoch of star formation in the population at 1.434 billion years old. This result supports the merger scenario where the companion galaxy and the galaxy pair formed seperately, perhaps with the companion forming at a relatively more recent time than the galaxy pair. After a time, the companion galaxy passed through the pair, driving gas inflow and a large increase in star formation. This also leaves the tidal features present in Figure 1a.

Another interesting feature of this system is the contrast in emission lines of the galaxy pair spectra.

Figure 8 shows the spectra of the pair nuclei from the SDSS. Clearly, pair B has substantial emission, while pair A does not. This corresponds with results from the FIRST survey shown in Fiugre 1b, which marks pair B as the most substantial radio source of the two. As mentioned, emmision lines can be caused either by star formation or AGN activity. Star formation seemed to be the clear choice, as stellar population synthesis suggested that pair B has substantial current star formation. For further evidence, the strengths of the emission lines were fit and compared by constructing a BPT diagram.

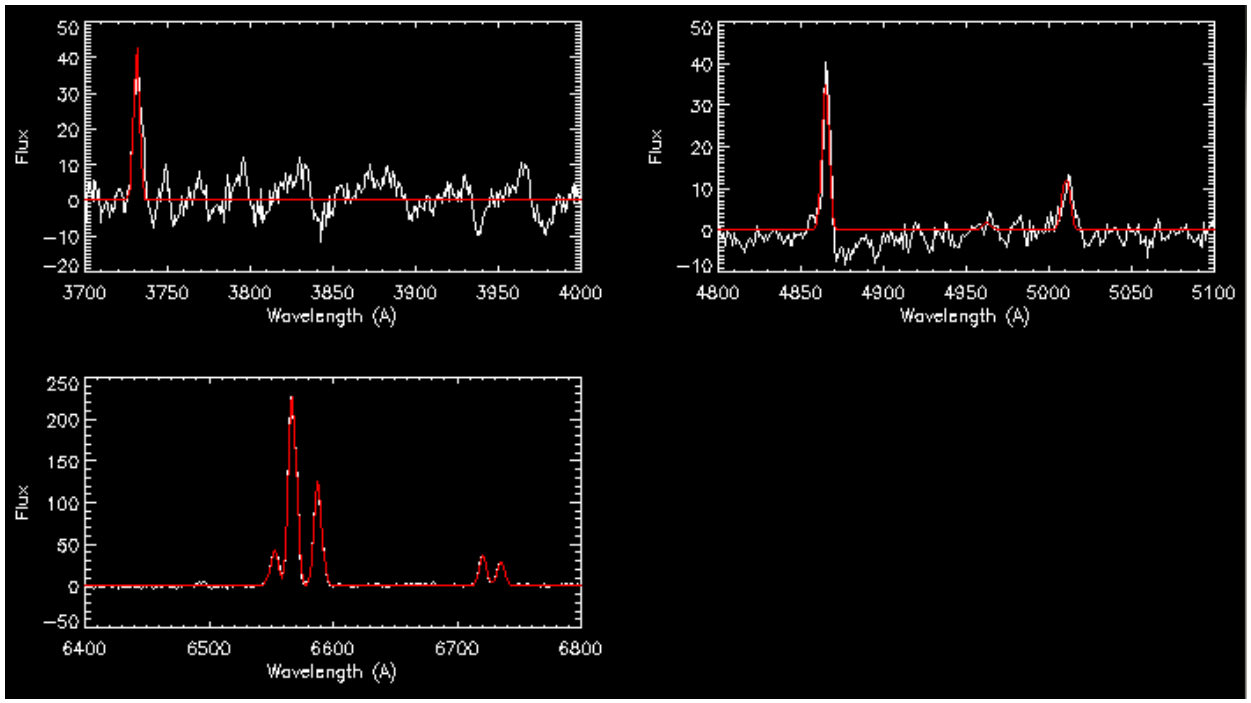

Figure 9: Output of emission fitting for SDSS Pair B.

Figure 9 shows an example of emission fitting using the SDSS Pair B spectrum. The relative flux of the Hα, Hβ, [OIII] λ5007, and [NII] λ6583 emission lines were measured for each spectrum, and the results are provided in Table 1. From these, a BPT diagram was constructed. This is shown in Figure 9. The two spectra that were centered mainly on pair B (fiber 48 and the SDSS nucleus) fall beneath Kauffmann's (2003) observational and Kewley's (2001) modeled constraints for star formation based emissions. The strength of the [NII] λ6583 emission line in fiber 31 puts it just outside Kewley's (2001) theoretical constraint. The companion galaxy is represented by fiber 60. Its placement on the BPT diagram puts it on the border between a case of emission caused by

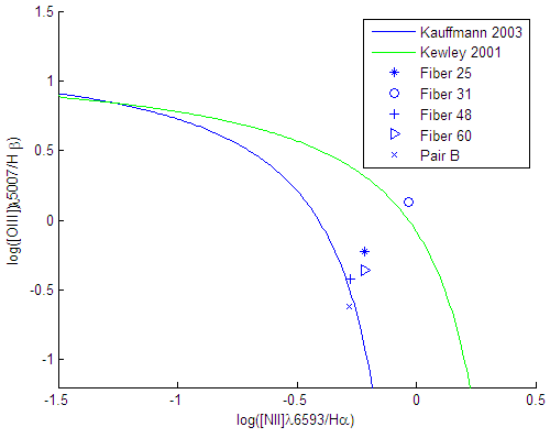

Figure 10: A BPT diagram using emission fitting results of the J075323 system.

Table 2: Velocity Results

	Velocity (km/s);			
	Na λ5890	Na λ5896	Ca K λ3934	Ca K λ3969
SDSS Pair A	-145.31	-137.29	-181.15	295.45
SDSS Pair B	113.967	67.71	-100.52	N/A

star formation and emission caused by AGN. Recalling the results from the FIRST (Figure 1b) and NVSS radio surveys, the galaxy is an extended radio source and has a potential variability, both of which lend credence to AGN activity contributing to the emission.

To test for possible gas outflows, we analyzed the velocities of the sodium doublet absorption lines from the gaseous interstellar medium and calcium H and K absorption lines from . These lines are redshifted by ∼3 Å, which indicates velocity of some kind. A significant difference (∼500 km/s) between the sodium and calcium lines would be a strong indicator of gas outflows. These results are shown in Table 2 for the SDSS spectrum pair A. With velocity differences on the order of 100-200 km/s, these results rule out gas outflow as the catalyst for blueshifted absorption features, leaving galactic velocity structure as the probable cause.

6.2 J233917

Figure 13 shows the stellar population snythesis results for each spectrum from J233917, which includes four fibers from SparsePak and the nucleus spectrum from SDSS. Each spectrum points

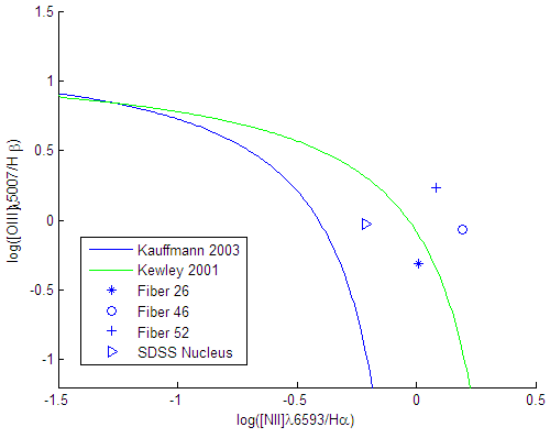

Figure 11: A BPT diagram using emission fitting results of the J233917 system.

towards its particular area of observation on an image of the galaxy overlaid with the SparsePak fiber map. Table **??** yields the percentage of total light produced by the model stellar populations for each spectrum. This system has a recent epoch of star formation on top of an older population indicitive of a post-starburst. However, the younger star formation period for this galaxy is shown by significant stellar populations at 1434 million years and 2500 million years, decidedly older than that of the J075323 system. The fit of the nucleus spectrum provided by the SDSS yields a small stellar population of 6.5 percent light produced in the 5.01 million year range, providing a small amount of evidence for current star formation. Lack of young stellar populations in the surrounding fibers pointed towards a nuclear starburst.

To determine whether the emission lines and potentially the radio emission was due primarily to star formation or AGN activity, we used emission line fitting. Figure 11 shows the BPT diagram for J233917. Fiber 26 and the SDSS nucleus spectrum are both outside the observational constraints set by Kauffmann (2003) and just inside the theoretical boundary of Kewley (2001). However, fiber 46 and fiber 52 are beyond both sets of constraints. These results suggest that J233917 may house a partially active AGN that is producing substantial emission lines and radio signal.

7 Significance

Little analysis on the observational data for the post-starburst galaxies with active AGN in the radio spectrum has been done. As such, our results significantely contribute towards efforts to distinguish possible causes of this activity. In a larger sense, the stellar population synthesis of the galaxies provides data that will help put more precise obervational constraints on the lifetime of post-starbursts.

8 Conclusions

Stellar population synthesis yielded comparable significant populations of recent star formation in both the galaxy pair and the companion in system J075323. This result, combined with the highly disturbed morphology of the galaxy pair and extended tidal features present in the optical image of the system provides a compelling case for a scenario in which the pair and companion gravitationally interacted in the past. This interaction caused staburst in both pair A and the companion, while pair B continues to have ongoing star formation. Emission line analysis for pair B suggests that its emission is caused by star formation, rather than AGN activity. While results for the companion galaxy suggest a combination of star formation and AGN activity. Furthermore, the extended radio emission and potential variability of the galaxy suggest an AGN. Finally, there is no evidence of gas outflows for the system. For the galaxy J233917, stellar population synthesis produced a picture indicative of an older nuclear starburst. For this system, emission line analysis suggests AGN activity as the source of emission. Thus, J233917 appears to be a non-merger post-starburst galaxy housing a mild AGN.

9 Future Work

Recent observations of the J075323 system using the WIYN High Resolution Infrared Camera (WHIRC) will be used to determine the dust extinction of the system, which can be used to constrain that parameter during stellar population synthesis, possibly improving results. Additionally, the near-infrared data will supply information about the system's metallicity, which can be used to

break the age-metallicity degeneracy of the stellar population synthesis results.

10 References

Baldwin J. A., Phillips M. M., Terlevich R., 1981, PASP, 93, 5

Bershady M. A., Andersen R. A., Harker J., Ramsey L. W., Verheijen M. A. W., 2004, PASP, 116,565

Bower R. G., Benson A. J., Malbon R., Helly J. C., Frenk C. S., Baugh C. M., Cole S., Lacey C. G., 2006, MNRAS, 370, 645

Bruzual G., Charlot S., 2003, MNRAS, 344, 1000

Chang T., van Gorkom J. H., Zabludoff A. I., Zaritsky D., Mihos J. C., 2001, AJ, 121, 1965

Croton D. J., et al., 2006, MNRAS, 365, 11

Goto T., 2007, MNRAS, 381, 187

Granato G. L., De Zotti G., Silva L., Bressan A., Danese L., 2004, ApJ, 600, 580 Hopkins P. F., Hernquist L., Cox T. J., Di Matteo T., Robertson B., Springel V., 2006, ApJS, 163, 1

Hopkins P. F., Hernquist L., Cox T. J., Keres D., 2008, ApJS, 175, 356

Kauffmann G., Heckman T. M., Tremonti C., et al., 2003, MNRAS, 346, 1055

Kewley L. J., Dopita M. A., Sutherland R. S., Heisler C. A., Trevena J., 2001, ApJ, 556, 121

Liu C. T., Hooper E. J., O'Neil K., Thompson D., Wolf M., Lisker T., 2007, ApJ, 658, 249

Norton S. A., Gebhardt K., Zabludoff A. I., Zaritsky D., 2001, ApJ, 557, 150

Oegerle W. R., Hill J. M., Hoessel J. G., 1991, ApJ, 381, L9

Poggianti B. M., Smail I., Dressler A., Couch W. J., Barger A. J., Butcher H., Ellis R. S., Oemler A. J., 1999, ApJ, 518, 576

Pracy M. B., Couch W. J., Blake C., Bekki K., Harrison C., Colless M., Kuntschner H., de Propris R., 2005, MNRAS, 359, 1421

Pracy M. B., Owers M. S., Couch W. J., Kuntschner H., Bekki K., Briggs F., Lah P., Zwaan M., 2012, MNRAS, 420, 2232

Thacker R. J., Scannapieco E., Couchman H. M. P., 2006, ApJ, 653, 86

Trioulle L., Barger A. J., Tremonti C., 2011, ApJ, 742, 46

Snyder G. F., Cox T. J., Hayward C. C., Hernquist L., Jonsson P., 2011, ApJ, 741, 77

Springel V., Di Matteo T., Hernquist L., 2005, ApJ, 620, L79

Yamauchi C., Goto T., 2005, MNRAS, 359, 1557

Yang Y., Zabludoff A. I., Zaritsky D., Mihos J. C., 2008, ApJ, 688, 945

Zabludoff A. I., Zaritsky D., Lin H., Tucker D., Hashimoto Y., Shectman S. A., Oemler A., Kirshner R. P., 1996, ApJ, 466, 104

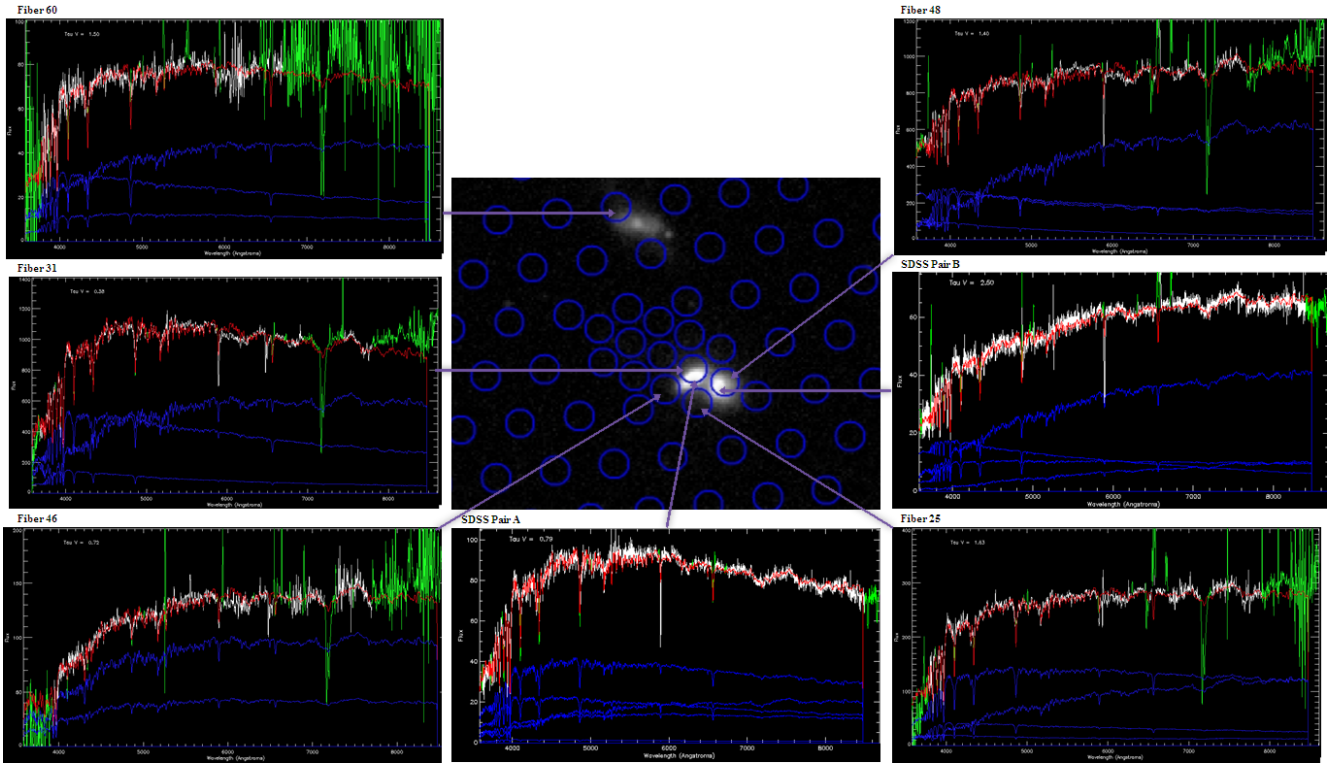

Figure 12: Stellar population synthesis results for the J075323 system. At the centre is the system image overlaid with the SparsePak fiber map.

Table 3: Stellar population synthesis results for the J075323 system.

	Stellar Population Age (Myr)									
	5.01	25.12	101.52	286.12	640.54	904.79	1434	2500	5000	10000
	Percentage of Total Light									
Fiber 25	0	5.21	0	12.85	50.78	0	0	0	0	31.56
Fiber 31	0	0	0	8.55	39.09	0	0	0	0	52.36
Fiber 46	0	0	0	0	0	0	0	31.03	68.97	0
Fiber 48	5.26	21.14	0	22.52	0	0	0	0	0	51.07
Fiber 60	0	0	0	32.07	15.4	0	52.53	0	0	0
SDSS Pair A	0	0	0	1.19	21.81	42.36	15.29	0	0	19.35
SDSS Pair B	20.34	0	0	17.84	0	0	52.126	0	0	9.69

Table 4: Stellar population synthesis results for the J233917 system.

	Model Star Age (Myr)									
	5.01	25.12	101.52	286.12	640.54	904.79	1434	2500	5000	10000
	Percentage of Total Light									
Fiber 26	0	1.08	0	0	36.08	0	0	55.02	0	7.82
Fiber 46	0	0	0	0	0	1.39	30.10	0	0	68.51
Fiber 47	0	0	0	0.70	0	0	69.71	0	0	29.59
Fiber 52	0	0	0	0	0	9.22	0	24.20	0	66.58
SDSS Nucleus	6.50	0	0	0	0	1.03	75.47	0	0	17.01

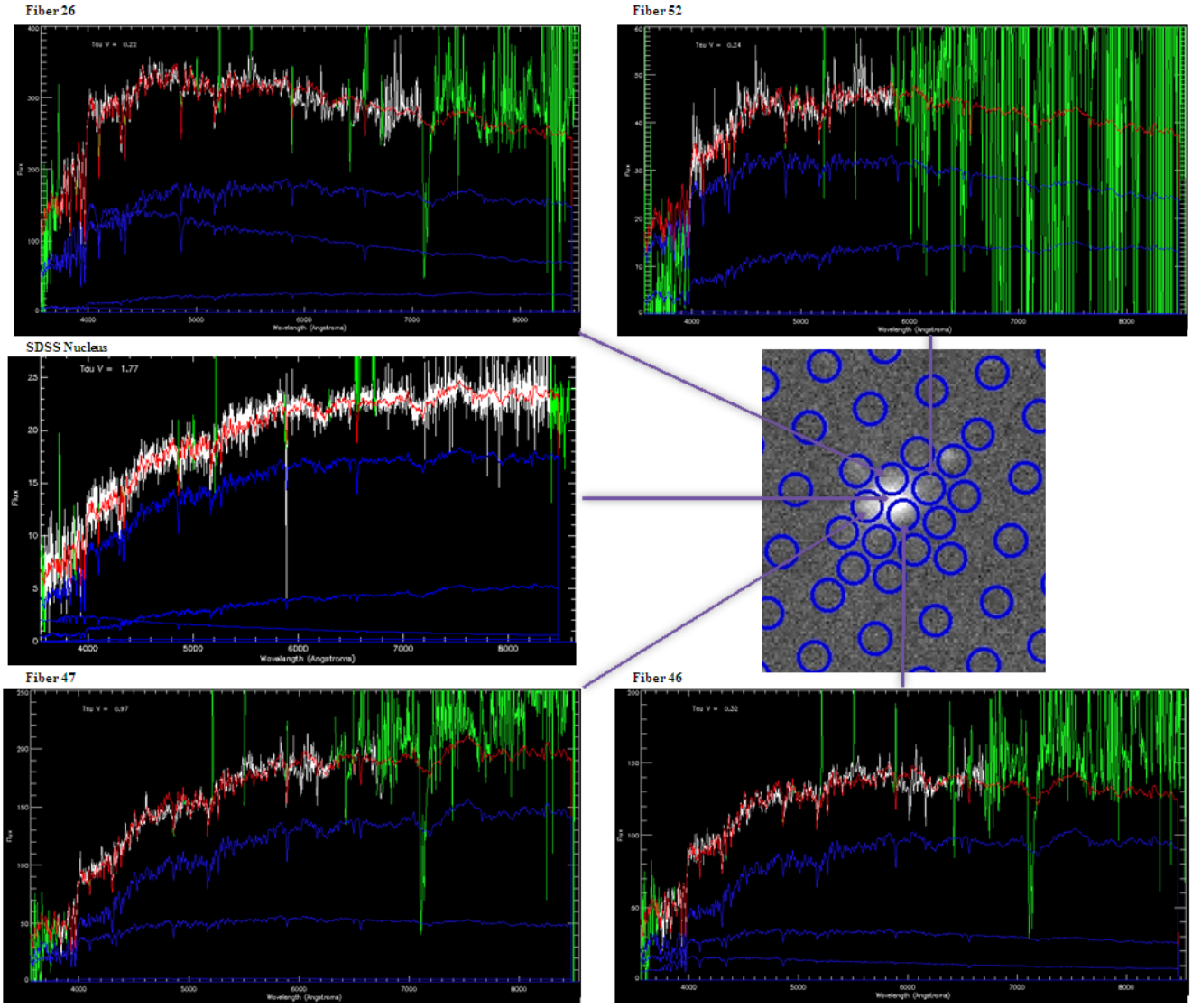

Figure 13: Stellar population synthesis results for the J233917 system. The system image overlaid with the SparsePak fiber map is to the middle right.